Journal of
Microscopy

Journal of Microscopy, Vol. 250, Pt 2 2013, pp. 111–115
Received 11 September 2012; accepted 10 February 2013
doi: 10.1111/jmi.12026

Qualitative microanalysis of calcium local structure in tooth layers by means of micro-RRS

J.J. LEANI*, H.J. SÁNCHEZ*,†, M.C. VALENTINUZZI*,†, C. PÉREZ‡ & M.C. GRENÓN§
*Facultad de Matemática Astronomía y Física, Universidad Nacional de Córdoba, Córdoba, Argentina
†CONICET, República, Argentina
‡Laboratorio Nacional de Luz Síncrotron, Campinas, Brazil
§Facultad de Odontología, Universidad Nacional de Córdoba, Córdoba, Argentina

Key words. Synchrotron radiation, X-ray microanalysis, XRF.

Summary

The Resonant inelastic X-ray scattering or resonant Raman scattering is an inelastic process of second order that becomes important when the energy of the excitation radiation is below but close to an absorption edge. In this process, the emitted photons have a continuous energy distribution with a high energy cut-off limit. In the last few years, experiments of resonant Raman scattering has become a very powerful technique to investigate excitations of electrons in solids. A qualitative study of the calcium local structure in the different layers of teeth was carried out. In order to perform the analysis, several measurements of tooth samples were achieved using monochromatic synchrotron radiation at the XRF station of the D09B-XRF beamline at the Brazilian synchrotron facility (LNLS, Campinas), below and close to the K absorption edge of Ca to inspect the resonant Raman scattering spectra. First of all, the spectra were analyzed with specific software to fit the experimental data. After that, the residuals were determined and a fast Fourier transform smoothing procedure was applied, taking into account the instrument functions of the detecting system. These oscillations present patterns that depend of the tooth layer, i.e. of the calcium state.

Introduction

When atoms are irradiated by X-ray photons different kinds of interactions take place: the photon can be absorbed by the photoelectric effect or can suffer a Rayleigh or Compton scattering. However, under resonant conditions, other low-probability interactions can occur. One of these interactions is the resonant Raman scattering (RRS, Karydas & Paradellis, 1997).

Correspondence to: Héctor Jorge Sánchez, Facultad de Matemática Astronomía y Física, Universidad Nacional de Córdoba, 5000 Córdoba, Argentina. Tel: +54-351-4334051; fax: +54-351-4334051; e-mail: jsan@famaf.unc.edu.ar

The X-ray RRS is an inelastic scattering process which presents fundamental differences compared to other scattering interactions between X-rays and atoms; when the energy of the incident photon approaches from below to the absorption edge of the target element, a strong resonant behaviour takes place contributing to the attenuation of X-rays in matter.

A theoretical description of the RRS process is given by the Kramers–Heisenber equation in time depending perturbation theory:

$$H_{int} = \sum_j \frac{e^2}{2mc^2} \boldsymbol{A}_j^2 - \sum_j \frac{e}{mc} \boldsymbol{p}_j . \boldsymbol{A}_j ,$$

where $\boldsymbol{p}_j$ is the momentum of the jth target electron and $\boldsymbol{A}_j$ the vector potential of the electromagnetic field. The $\boldsymbol{A}_j^2$ term is responsible for scattering (including diffraction and nonresonant inelastic scattering), whereas the $\boldsymbol{p}_j.\boldsymbol{A}_j$ term is related to the absorption processes and resonant scattering. Depending on the energy and the momentum transfer in the inelastic scattering process, quite distinct information can be obtained. According to the absorption-emission model, the RRS process can be described with an initial state, an intermediate state and a final state (Sánchez *et al.*, 2006). The initial state consists on an incident photon with energy below the absorption threshold energy. In the intermediate state, a hole is produced in an inner shell and the excited electron is ejected to an unoccupied state; an electron from a higher shell fills the vacancy and a photon is emitted. The final state consists of a hole in a higher shell, a scattered photon and an excited electron (in the continuum or in a bound excited state).

Supposing a well-defined energy of the incident photon, the energy conservation for the scattering process leads to (Rubensson, 2000)

$$E_0 - \Omega_L - E_f = E_S + k_e ,$$

where E_0 the incident photon energy, Ω_L the energy of the L threshold, E_f the Fermi energy, E_S the energy of the scattered photon and k_e the kinetic energy of the excited electron. This

expression tells us that between the initial and final states the available energy has to be shared between the excited electron and the emitted photon.

This paper presents first results of determination of the calcium oxidation state in several tooth layers by means of RRS spectroscopy using monochromatic synchrotron radiation with an energy dispersive system.

The spectra were analyzed with dedicated programs for fitting nonconventional curves to the experimental data and a fast Fourier transform smoothing procedure was applied. After the smoothing process, the RRS residuals were studied in order to identify the resultant variations. Since the chemical bonding of an element affects the emission of the scattered photons; the final state of the excited electron affects its energy, then the variations in the Raman spectra are related with the chemical environment of the absorbing element, in this case calcium, and can supply significant structural information about biological samples.

Using an energy dispersive system, changes in the RRS structure were observed, offering a new possibility of identifying both the elements present in a sample and their oxidation state in several kinds of samples (Kotani & Shin, 2001; Karydas *et al.*, 2002). Recently, it has been successfully employed X-ray Raman scattering spectroscopy to determine oxidation states of metals (Leani *et al.*, 2011a,b).

The authors want to clarify that the results in this work do not take into account photoelectron bremstralung contribution to the background. The contribution of this process is most important in low-energy region and does not affect significantly the range of the scattered line (Bannett *et al.*, 1977). Besides, the bremstralung is a smooth and continuous energy function that does not interfere with the faster variations in the spectra that are investigated in this work. Moreover, the bremstralung effect has the same energy distribution in all the studied samples, being compensated in the spectral comparison.

The aim of this work is to introduce a new technique that allows structural characterizations in biological samples using emission spectroscopy. It is focused on the potential (in terms of spatial resolution) of a new spectrometric technique. The samples were selected to illustrate this potential (Abraham *et al.*, 2007). Although it could present a low count rate in some experimental conditions (e.g. incident energy too far away from K-absorption edge energy) its emission condition allows, modifying irradiation and/or detection conditions, employ this technique in geometries impossible to achieve with conventional absorption techniques.

Measurements and data processing

The measurements were carried out in XRF station of the D09B-XRF beamline (Pérez *et al.*, 1999) at the Brazilian synchrotron facility (LNLS). This synchrotron light source operates at a nominal energy of 1.37 GeV with a maximum current of 250 mA in multibunch mode, emitting photons with a critical energy of 2.08 keV. The XRF beamline is equipped with a double crystal 'channel-cut' monochromator, the energy resolution of the monochromator is ∼3 eV at 10 keV using a Si(111) crystal. For the measurements performed in this work, the incident beam was collimated with orthogonal slits in order to obtain over the sample a spot of 400∗500 micrometres and monitored with ionization chambers, resulting in a flux on the sample of $\sim 10^8$ ph s^{-1} @ 10 keV. The detection systems are energy-dispersive set-ups composed by several solid-state detectors with different windows and different electronic chains. The detector used in this work was an Ultra-LEGe solid-state detector with a Be windows of 8 μm and an energy resolution of 158 eV for the Mn-Kα line. Pulse processing was accomplished by a fast amplifier with triangular shaping and spectra were processed and collected with a 8K multichannel analyzer. The experimental geometry was the typical $45^\circ + 45^\circ$ configuration on the electron orbit plane to reduce Compton and Rayleigh scattering; the measurements were carried out in air atmosphere, taking into account the air absorption.

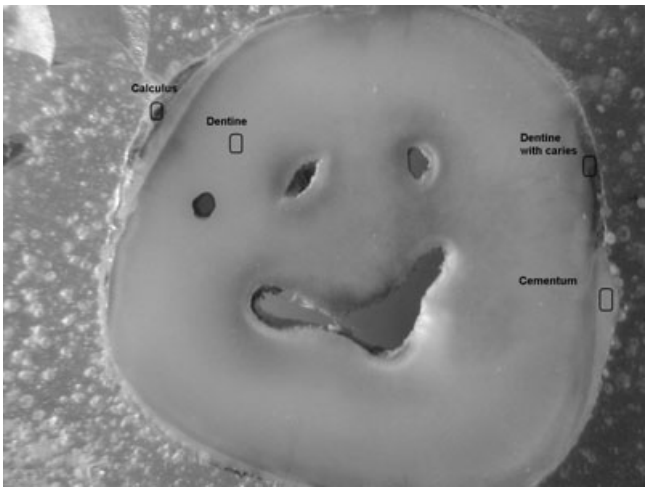

Fig. 1. The thin sample: a transversal cut of human tooth of ∼1 mm embed in light matrix. It is possible to see the four measured points in the graphic.

The samples consisted in transversal cuts of human teeth embed in light matrix with thickness of ∼1 and ∼4 mm (Figs 1 and 2, respectively). These samples were irradiated in four different layers: dentine, dentine with caries, cementum and external calculus in the case of the thin tooth (see Fig. 1), two different dentine positions, enamel and external calculus (with a small enamel contribution) in the case of the thick sample (see Fig. 2).

These layers were irradiated with monochromatic photons of 3950 eV, i.e. 88.5 eV below the Ca K-edge to inspect the Raman emissions. The measuring livetime was 12 000 s per

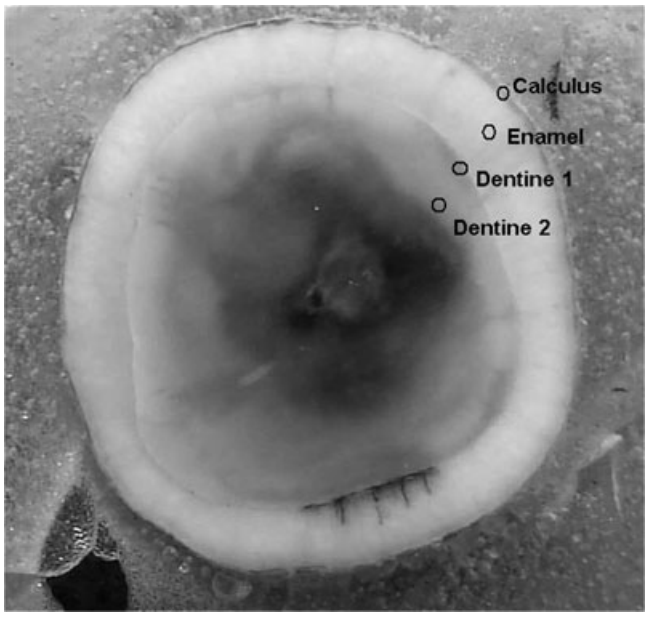

Fig. 2. The thick sample: a transversal cut of human tooth of ~4 mm embed in light matrix. It is possible to see the four measured points in the graphic.

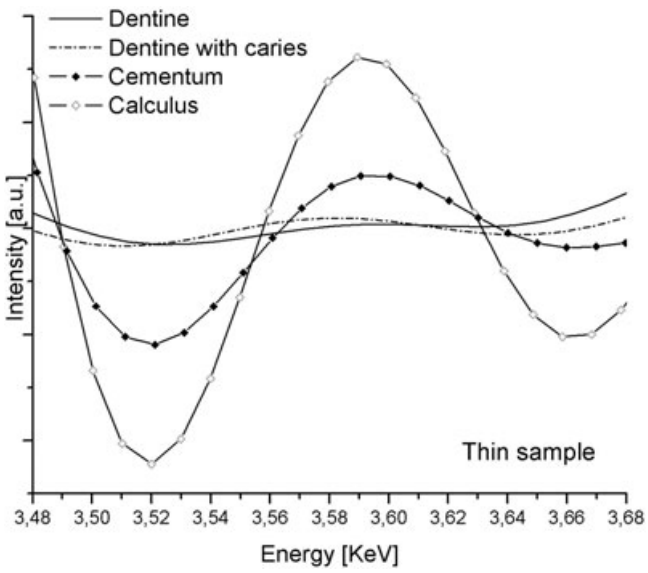

Fig. 3. Residuals between the experimental Raman spectra and data fitting for the four different tooth layers in the case of the thin sample (see Fig. 1).

point in the case of the thin sample and 10 000 s per point in the case of the thick tooth.

The resulting spectra were analyzed with conventional programs for spectrum analysis (TableCurve, 1993; PeakFit, 2003) using nonlinear functions for data fitting.

The low energy side (starting just in the centre of the peak) of Raman peaks were fitted using logistic functions:

$$y = \frac{a_0 \exp\left(-\frac{x-a_1}{a_2}\right)}{a_2\left[1+\exp\left(-\frac{x-a_1}{a_2}\right)\right]^2}, \qquad (1)$$

where a_0 is the area of the peak, a_1 is its centre and a_2 is the width of the distribution. Logistic expressions were selected by the used software (TableCurve, 1993) among almost 3000 possible theoretical expressions for fitting of the data, possibly because it fits with high accuracy ($r2 > 0.999$) also the low-energy tail of the inelastic peaks. This high level of precision is crucial in order to be certain that residuals between theoretical model and the experimental spectrum provide physical information and not be originated by an incorrect fitting.

A standard denoising method was employed based on the frequency decomposition of the signal (Zhang *et al.*, 2006). After the theoretical fitting, a fast Fourier transform smooth procedure was applied to the experimental spectra considering a Gaussian instrumental function with a σ of 67 eV. The smoothing is accomplished by removing Fourier components with frequencies larger than $(1/n\Delta t)$ where n is the number of data points considered at a time and Δt is the time spacing between two adjacent data points. By suppressing the high-frequency components, the noise associated with them can be eliminated. It works as a perfect lowpass filter where the cut-off frequency plays the role of a parameter during the analysis.

This kind of filter offers a very important physical sense at the moment of inspecting the experimental data, in opposition to the methods that are purely mathematics (e.g. methods based in pondered averages).

It should be noted that the data analysis is relatively simple and direct, in comparison with the data treatment required for other techniques. This simplicity, in addition to the low number of steps to reach the final result, turns this analysis into a sensitive procedure. In addition, previous results and theoretical background indicate a significant degree of reliability. Regarding the property or characteristic of the RRS residual curve as representative of the different species, there is not a detailed theory of the resonant Raman (second order) interaction yet. It has been suggested that the RRS curves could be associate with extended X ray analysis fine structure curves but this has not been proven yet.

Results and discussions

As it should be expected, the Raman scattering process is resonantly enhanced as the energy of the incident photons becomes closer to the Ca-K absorption threshold; in addition, the Raman peak is more intense, dominating over the Compton peak.

The low-energy residuals (just below of Raman peaks centre) between the theoretical expression (1) and the experimental spectra, after the smoothing procedure, are shown in Figures 3 and 4 for the thin and thick teeth, respectively.

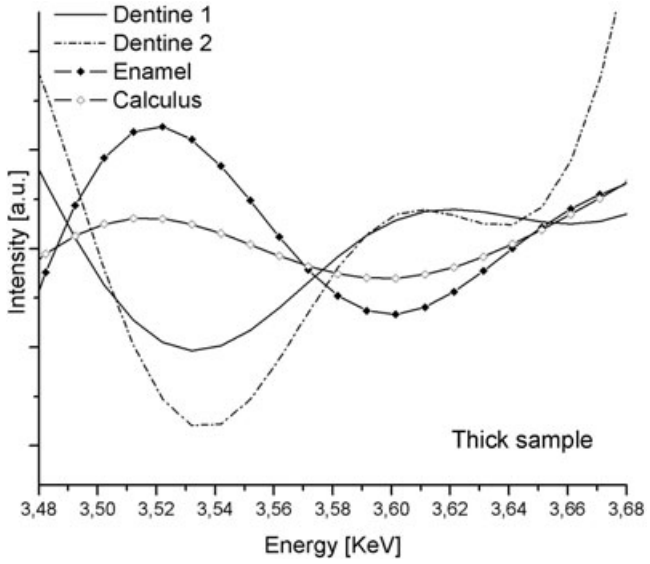

Fig. 4. Residuals between the experimental Raman spectra and data fitting for the four different tooth layers in the case of the thick sample (see Fig. 2).

These curves show a certain degree of similarities, because in general teeth structures are mainly composed by different octocalcium phosphates. Nevertheless, small changes in the oscillation patterns (like positions of peaks, small changes in frequency, number of 'valleys', etc.) allows to characterize discriminate the different tooth layers, which correspond to different structures.

As can be appreciated, the RRS residuals of calcium from the layers are different between them; however, in the case of the thick tooth, residuals from the enamel and external calculus layers present a similar oscillation pattern. An analogous behaviour could be appreciated from the two dentine positions. On the other hand, the thin sample presents similarities in the oscillation patterns of dentine layers and also between the cementum and calculus residuals.

In addition, the dentine layers present in both samples studied present similar oscillation patterns between them. Note the 'valleys' at 3.53 and 3.64 keV and the peak at 3.62 keV. These results show that residuals expose chemical environment information and it is not a mere fitting artefact.

Although the main presence of calcium in teeth is by means of hydroxyapatite, the similarities of the oscillation patters observed in the results suggest that other calcium phases (whitelokite, brushite, calcium carbonates and even octocalcium and tricalcium phosphates) could be also present.

Furthermore, the hydroxyapatite is a very flexible molecule, so, depending on the molecule environment, changes in the RRS residuals due to contributions of different interference effects could be also possible.

This work is pioneer in the area and an important work of interpretation is necessary in the future. In addition, biological samples present an extra complexity since the studied element could be there in several states simultaneously. Nevertheless, the behaviour observed in the residuals could be used to recognize the local structure of elements in biological samples under study, offering a possibility of chemical environment determination using RRS spectroscopy.

Conclusions

The capability of the RRS technique to discriminate different oxidation states or crystalline structures has been largely demonstrated in several papers (see References in the manuscript). Due to the physics basis of the technique, this capability is valid for any element of the periodic table. Although these measurements do not specify the oxidation state in the different points under measurement the clear variations of the RRS spectra are strong evidence of changes in the Ca structure along the measuring path. Considering that the RRS technique is a novel method under development, the obtained results fulfils the aims of the paper.

The results shown above point out the existence of a clear difference among the different layers of the measured samples, i.e. the calcium local structure. These results suggest the possibility of structural characterization by means of RRS using an energy-dispersive system combined with synchrotron radiation.

An RRS chemical environment technique will offer an opportunity to study the oxidation state of different kind of samples, such as mineral, environmental and/or biological samples, or samples in which a complete characterization is impossible to achieve by other methods, such as conventional absorption techniques. Further investigations and measurements are currently carried out in order to reach a better understanding of the processes involved and the implementation of a practical procedure.

Acknowledgement

This work has been partially supported by the Brazilian Synchrotron Light Laboratory (LNLS)/Brazilian Biosciences National Laboratory (LNBio).

References

Abraham, J.A., Grenón, M.S., Sánchez, H.J., Valentinuzzi, M.C. & Perez, C.A. (2007) μXRF analysis of traces and calcium-phosphate phases on tooth-tartar interfaces using synchrotron radiation. *Spectrochim. Acta B* **62**, 689–694

Bannett, Y., Rapaport, D. & Freund, I. (1977) Resonant x-ray Raman scattering and the infrared divergence of the Compton effect. *Phys. Rev. A* **16**, 2011–2021.

Karydas, A.G., Galanopoulos, S., Paradellis, T. & Kallithrakas-Kontos, N. (2002) Chemical state speciation by resonant Raman scattering. *J. Phys.: Condens. Matter* **14**, 12367–12381.

Karydas, A.G. & Paradellis, T. (1997) Measurement of KL and LM resonant Raman scattering cross sections with a proton-induced CrKα x-ray beam. *J. Phys. B* **30**, 1893–1905.

Kotani, A. & Shin, S. (2001) Resonant inelastic x-ray scattering spectra for electrons in solids. *Rev. Mod. Phys.* **73**, 203–246.

Leani, J.J., Sánchez, H.J., Valentinuzzi, M.C. & Pérez C. (2011a) Determination of the oxidation state by resonant-Raman scattering spectroscopy. *J. Anal. At. Spectrom.* **26**, 378–382.

Leani, J.J., Sánchez, H.J., Valentinuzzi, M.C. & Pérez C. (2011b) Chemical environment determination of iron oxides using RRS spectroscopy. *X-Ray Spectrom.* **40**, 254–256.

PeakFit v4.12 for Windows. (2003) SeaSolve Software Inc., Portions Copyright 2000–2003 SYSTAT Software Inc.

Pérez, C.A., Radke, M., Sánchez, H.J., *et al.* (1999) Synchrotron radiation X-ray fluorescence at the LNLS: beamline instrumentation and experiments. *X-Ray Spectrom.* **28**, 320–326.

Rubensson, J. (2000) RIXS dynamics for beginners. *J. Electron Spectrosc. Relat. Phenom.* **110–111**, 135–151.

Sánchez, H.J., Valentinuzzi, M.C. & Pérez C. (2006) X-ray resonant Raman scattering cross sections of Mn, Fe, Cu and Zn. *J. Phys. B* **39**, 4317–4327.

TableCurve v1.11 for Windows. (1993) AISN Software.

Zhang, Q., Aliaga-Rossel, R. & Choi, P. (2006) Denoising of gamma-ray signals by interval-dependent thresholds of wavelet analysis. *Meas. Sci. Technol.* **17**, 731–735.